

## MIT Open Access Articles

*Synergistically Chemical and Thermal Coupling between Graphene Oxide and Graphene Fluoride for Enhancing Aluminum Combustion*

The MIT Faculty has made this article openly available. **Please share** how this access benefits you. Your story matters.

**Citation:** Jiang, Yue et al. "Synergistically Chemical and Thermal Coupling between Graphene Oxide and Graphene Fluoride for Enhancing Aluminum Combustion." ACS Applied Materials and Interfaces 12, 6 (January 2020): 7451–7458 © 2020 American Chemical Society

**As Published:** <http://dx.doi.org/10.1021/acsami.9b20397>

**Publisher:** American Chemical Society (ACS)

**Persistent URL:** <https://hdl.handle.net/1721.1/127994>

**Version:** Author's final manuscript: final author's manuscript post peer review, without publisher's formatting or copy editing

**Terms of use:** Creative Commons Attribution-Noncommercial-Share Alike



# 1 Synergistically Chemical and Thermal Coupling between Graphene Oxide and Graphene Fluoride for Enhancing Aluminum Combustion

3 Yue Jiang,<sup>#</sup> Sili Deng,<sup>#</sup> Sungwook Hong,<sup>#</sup> Subodh Tiwari, Haihan Chen, Ken-ichi Nomura,  
4 Rajiv K. Kalia, Aiichiro Nakano, Priya Vashishta, Michael R. Zachariah, and Xiaolin Zheng\*



Cite This: <https://dx.doi.org/10.1021/acsami.9b20397>



Read Online

ACCESS |



Metrics & More



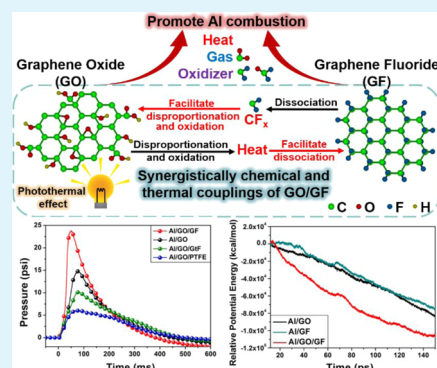
Article Recommendations



Supporting Information

5 **ABSTRACT:** Metal combustion reaction is highly exothermic and is used in energetic  
6 applications, such as propulsion, pyrotechnics, powering micro- and nano-devices, and  
7 nanomaterials synthesis. Aluminum (Al) is attracting great interest in those applications  
8 because of its high energy density, earth abundance, and low toxicity. Nevertheless, Al  
9 combustion is hard to initiate and progresses slowly and incompletely. On the other  
10 hand, ultrathin carbon nanomaterials, such as graphene, graphene oxide (GO), and  
11 graphene fluoride (GF), can also undergo exothermic reactions. Herein, we  
12 demonstrate that the mixture of GO and GF significantly improves the performance  
13 of Al combustion as interactions between GO and GF provide heat and radicals to  
14 accelerate Al oxidation. Our experiments and reactive molecular dynamics simulation  
15 reveal that GO and GF have strong chemical and thermal couplings through radical  
16 reactions and heat released from their oxidation reactions. GO facilitates the  
17 dissociation of GF, and GF accelerates the disproportionation and oxidation of GO.  
18 When the mixture of GO and GF is added to micron-sized Al particles, their synergistic  
19 couplings generate reactive oxidative species, such as  $CF_x$  and  $CF_xO_y$ , and heat, which greatly accelerates Al combustion. This work  
20 demonstrates a new area of using synergistic couplings between ultrathin carbon nanomaterials to accelerate metal combustion and  
21 potentially oxidation reactions of other materials.

22 **KEYWORDS:** energetic materials, graphene oxide, graphene fluoride, flash ignition, aluminum combustion



## 1. INTRODUCTION

23 Combustion of metal-based energetic materials is an  
24 exothermic process that generates heat, light, and thrust  
25 rapidly, and it is of great interest for a variety of applications  
26 ranging from aerospace to nanoscale, including propulsion,  
27 pyrotechnics, micro- and nano-devices in microelectromechanical  
28 systems, and synthesis of nanomaterials.<sup>1–5</sup> Aluminum  
29 (Al) is the most popular metal for those applications due to its  
30 earth abundance, low toxicity, and high specific energy  
31 density.<sup>6</sup> In those applications, Al is typically used in the  
32 forms of nano- or micron-sized particles. Nano-sized Al (n-Al)  
33 has a lower ignition temperature and higher reactivity than the  
34 micron-sized Al ( $\mu$ -Al),<sup>7,8</sup> but n-Al tends to agglomerate and  
35 has a larger fraction of inert  $Al_2O_3$ . For example, a 50 nm  
36 diameter n-Al particle has about a 2 nm thick  $Al_2O_3$  shell,  
37 occupying 30% of the total n-Al mass. Hence,  $\mu$ -Al particles are  
38 still commonly used in practical applications.<sup>9,10</sup> It is highly  
39 desirable to improve the combustion performance of  $\mu$ -Al  
40 particles to be similar to n-Al for the aforementioned  
41 applications.

42 Recently, we have demonstrated that ultrathin graphene  
43 oxide (GO) lowers the ignition energy and increases the  
44 energy release rate of  $\mu$ -Al particles with a Xe lamp flash  
45 ignition.<sup>11</sup> The enhancement effect of GO is attributed to its

exothermic disproportionation and oxidation reactions, cata-  
46 lytic effects,<sup>11–14</sup> and excellent light absorption proper-  
47 ties.<sup>15–17</sup> In addition, we showed that the  $\mu$ -Al/GO composites  
48 exhibit much better combustion performance than the  $\mu$ -Al/  
49 metal oxides (e.g.,  $WO_3$ ) thermite mixtures with the same  
50 weight percentage of  $\mu$ -Al. Nevertheless, the addition of GO  
51 inevitably lowers the specific energy density of  $\mu$ -Al particles. It  
52 is desirable to increase the energy density of Al/GO while  
53 maintaining or even improving its combustion performance.

54 Fluorination of Al is known to have a much higher heat of  
55 reaction than that of Al oxidation (55.7 kJ/g vs 35.6 kJ/g).<sup>18</sup>  
56 Moreover, fluorine reacts with the native  $Al_2O_3$  layer to form  
57 more volatile  $AlF_3$ , which enhances both the ignition and the  
58 combustion of Al.<sup>19,20</sup> Hence, a potential solution for  
59 increasing the energy density of Al/GO is to replace some  
60 GO with fluorine-containing oxidizers. In fact, fluoropolymers,  
61 such as polytetrafluoroethylene (PTFE) and polyvinylidene  
62 fluoride, have been used as oxidizers and/or binders in Al-63

Received: November 10, 2019

Accepted: January 17, 2020

Published: January 17, 2020

64 based energetic composites or as surface-coating materials on  
65 Al particles to enhance their energetic performance.<sup>21–25</sup> In  
66 addition, graphite fluoride (GtF) was shown to enhance the  
67 combustion of Al and Mg particles.<sup>26,27</sup>

68 Here, we investigate a new type of fluorine-containing  
69 oxidizer, exfoliated monolayer graphene fluoride (GF),<sup>28,29</sup>  
70 and combine GF with GO to enhance the combustion performance  
71 of  $\mu$ -Al particles. GF is fully fluorinated graphene, and each  
72 carbon atom in the basal plane of GF is  $sp^3$  hybridized and  
73 bonded with one fluorine atom.<sup>30,31</sup> GF has a number of  
74 properties suitable for enhancing Al combustion. First, GF  
75 contains  $\sim 50$  at. % of fluorine, which is comparable to that of  
76 PTFE (66.6 at. %) and GtF ( $\sim 50$  at. %), but all those fluorine  
77 atoms in GF are exposed on the surface and easily accessible  
78 for reacting with Al. Secondly, GF, similar to GO, has a low  
79 density of  $\sim 2.7$  g/cm<sup>3</sup>,<sup>32,33</sup> so it helps to keep the specific  
80 energy density of the composite high. Finally, GF can be  
81 considered energetic as it decomposes and reacts with oxygen  
82 in the air at  $\sim 400$ – $600$  °C, generating  $CF_x$  and  $CF_xO_y$  species  
83 that can further react with Al.<sup>34,35</sup>

84 In this study, we experimentally and computationally  
85 compared the combustion performance of three mixtures:  $\mu$ -  
86 Al/GO,  $\mu$ -Al/GF, and  $\mu$ -Al/GO/GF. Motivated by our  
87 previous study on the enhanced optical ignition of  $\mu$ -Al by  
88 the intrinsic chemical activity of GO,<sup>11</sup> our current study used  
89 the chemical and/or thermal coupling effect of GO and GF to  
90 enhance the ignition and combustion of  $\mu$ -Al and further  
91 revealed the underlying mechanism responsible for the  
92 coupling effect of GO/GF. We found that the combination  
93 of GO and GF provides synergistic enhancements for  $\mu$ -Al  
94 ignition and combustion through both Xe flash ignition  
95 experiments and reactive molecular dynamics (RMD)  
96 simulation. The enhancement mechanism is schematically  
97 explained in Figure 1. GO is rapidly heated by the Xe flash

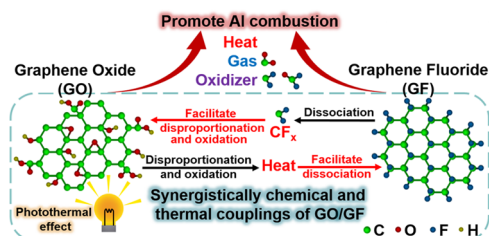


**Figure 1.** Proposed mechanism for GO/GF chemical and thermal couplings. Schematics of the synergistically thermal and chemical coupling between GF and GO and its effects for enhancing the energetic performance of Al (green, C atoms; red, O atoms; blue, F atoms; yellow, H atoms).

## 2. METHODS

**2.1. Material Preparation.** Al/GO/GF (80/10/10 wt %) 111  
composites were prepared by a mechanical mixing method. We first 112  
sonicated 10 mg of GO powder synthesized by the Hammer's method 113  
(0.5–5  $\mu$ m in diameter, 0.8–1.2 nm in thickness, XFNANO), and 10 114  
mg of GF powder prepared by high-temperature fluorination of 115  
graphene by  $F_2$  (0.4–5  $\mu$ m in diameter, 0.8 nm in thickness, 116  
XFNANO) in ethanol (1 mg/mL) for 2 h, separately. Then, the 117  
suspensions of GO and GF were mixed together, and the mixture was 118  
sonicated for another 1 h. Meanwhile, 80 mg of Al particles (3.0–4.5 119  
 $\mu$ m in diameter, Alfa Aesar) were dispersed in 8 mL of ethanol by 120  
sonication for 30 min. After that, the GO/GF suspension was added 121  
to the Al suspension and sonicated for 1 h. The mixture powders were 122  
collected by filtration and fully dried on a hotplate at 60 °C for 1 h 123  
and subsequently in a vacuum desiccator for 12 h. We used the same 124  
method to prepare other samples of GO/GF (50/50 wt %), Al/GO 125  
(80/20 wt %), Al/GF (80/20 wt %), Al/GO/GtF (80/10/10 wt %), 126  
and Al/GO/PTFE (80/10/10 wt %). The GtF powders are 4–10  $\mu$ m 127  
in diameter and 5–10 nm in thickness (XFNANO), and the PTFE 128  
powders are 100–200 nm in diameter (DuPont). 129

**2.2. Thermal Analysis of Samples with Thermogravimetry 130  
Analysis/Differential Scanning Calorimetry.** To investigate the 131  
thermal behaviors of GO and GF, the evolution of mass and heat flow 132  
of GO, GF, and GO/GF mixture heated in the air was investigated by 133  
the combination of thermogravimetry analysis and differential 134  
scanning calorimetry (TGA/DSC, Setaram LABSYS Evo). In each 135  
test, an alumina crucible of 100  $\mu$ L with 4 mg of the sample inside was 136  
heated at a rate of 10 °C/min from 100 to 800 °C in the air (40 137  
sccm). The baseline correction of the sample TGA and DSC curves 138  
was performed by subtracting the TGA and DSC curves of the empty 139  
alumina crucible with the same heating process. The heat release of 140  
each exothermic peak was obtained by integrating the peak area 141  
(illustrated as first  $\Delta H$  and second  $\Delta H$  in Figure 2b) of each DSC 142

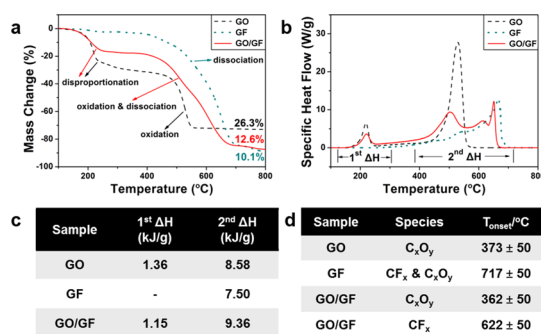


**Figure 2.** Thermal analysis of GO, GF, and GO/GF mixture showing the thermal and chemical couplings between GO and GF. (a) TGA and (b) DSC results of GO, GF, and GO/GF being heated from 100 to 800 °C at 10 °C/min in the air (the numbers labeled in (a) are the mass percentages of the residual materials after experiments); (c) specific heat release calculated by integrating the exothermic peaks labeled in (b) DSC curves of GO, GF, and GO/GF samples; (d) onset temperatures for the release of carbon oxide species  $C_xO_y$  (including  $CO_2$ ,  $CO$ ,  $C$ , and  $O$ ) and carbon fluorides species ( $CF_x$ ), measured by T-jump TOFMS experiments, which resistively heated the sample coated on a Pt filament to  $\sim 1000$  °C in 3 ms at  $2.0 \times 10^{-6}$  Torr.

curve. Similar TGA/DSC experiments were also conducted by heating 143  
5 mg of Al/GO (80/20 wt %) and Al/GO/GF (80/10/10 wt %) 144  
samples from 100 to 1250 °C to investigate their thermal behaviors. 145

**2.3. Temperature-Jump (T-Jump) Experiments.** GO, GF, and 146  
GO/GF mixture (50/50 wt %) were analyzed with a T-jump electron 147  
ionization mass spectrometer.<sup>39</sup> The electron energy was set at 70 eV. 148  
The sample was first dispersed in ethanol and sonicated for 1 h. It was 149  
then coated onto a Pt filament 76  $\mu$ m in diameter, which was 150  
resistively heated to  $\sim 1000$  °C in 3 ms at about  $2.0 \times 10^{-6}$  Torr near 151



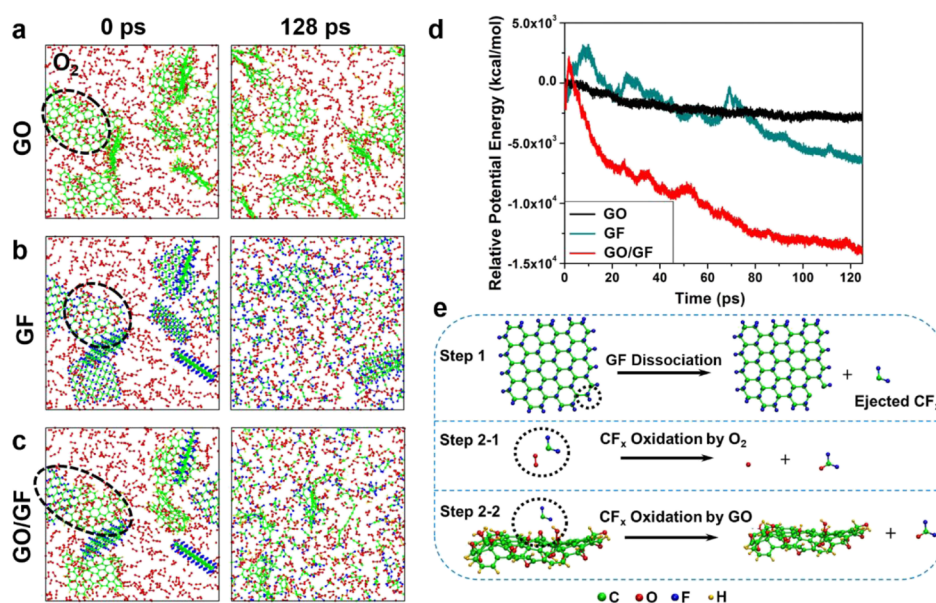


**Figure 3.** RMD simulation results reveal molecular-level thermal oxidation behaviors of GO, GF, and GO/GF mixture. Snapshots of RMD simulations for the thermal oxidation behavior of (a) GO, (b) GF, and (c) GO/GF 1:1 mixture with O<sub>2</sub> at 2000 K at 0 and 128 ps; (d) the relative potential energy vs time for the three different systems. A lower relative potential energy indicates more heat release; (e) reaction mechanisms for the oxidation of CF<sub>x</sub> species by O<sub>2</sub> molecule or GO, derived by RMD simulations (green, C atoms; red, O atoms; blue, F atoms; yellow, H atoms).

152 the ionization region of the mass spectrometer. The time-of-flight  
153 measurement was triggered by the T-jump heating pulse to measure  
154 the gas species released/generated from heating the filament. The  
155 temporal voltage and current of the T-jump probe were recorded  
156 during heating, allowing resistivity to be obtained and related to  
157 instantaneous temperature and mapped against mass spectra.

158 **2.4. RMD Simulation of Systems with and without Al.** We  
159 used the ReaxFF<sup>40,41</sup> reactive force field to investigate the chemical  
160 reactions of GO, GF, and Al with GO and GF. Because the entire  
161 system contains three different types of materials, multiple ReaxFF  
162 parameters were merged into a single force field (i.e., Al/C/H/O, C/  
163 H/F, and F–O interactions employed by Hong and van Duin,<sup>42</sup>  
164 Rahnamoun and van Duin,<sup>43</sup> and Kim et al.,<sup>44</sup> respectively). For  
165 RMD simulations, we modeled a pre-oxidized Al slab (5126 atoms), a  
166 single GO sheet (134 atoms), and a single GF sheet (136 atoms). We  
167 used an orthogonal simulation cell of 48.54 Å × 49.47 Å × 155.0 Å  
168 that contains the pre-oxidized Al slab model at the bottom, 16 GO/16  
169 GF sheets (or 16 GO/16 GF sheets without Al), and 2000 randomly  
170 distributed O<sub>2</sub> molecules. We applied a wall boundary condition in  
171 the z-direction of the simulation domain to prevent reactions between  
172 the bottom of the Al slab and gas species. The NVT ensemble (i.e., a  
173 constant number of atoms, a constant volume, and a constant  
174 temperature) with the Nosé–Hoover thermostat<sup>45,46</sup> was applied to  
175 the entire system. The detailed conditions of our RMD simulation can  
176 be found in our previous work.<sup>11</sup>

### 3. RESULTS AND DISCUSSION

177 **3.1. Experimental Comparison of Reaction Character-**  
178 **istics of GO, GF, and GO/GF Mixture in Air.** We first  
179 experimentally compare the reactive and thermal release  
180 properties of GO, GF, and GO/GF mixtures in the air in  
181 the absence of Al. Those properties were determined under  
182 both a slow heating rate (10 °C/min) using TGA and DSC  
183 and under a high heating rate (>10<sup>5</sup> °C/s) using the T-jump  
184 electron ionization mass spectrometer.<sup>39</sup> The TGA/DSC  
185 results are shown in Figure 2a–c, and the T-jump results are  
186 shown in Figure 2d. Under the slow heating condition, as  
187 shown in Figure 2a–c, pure GO first undergoes disproportion-  
188 ation reaction at 200 °C and is further oxidized at 500  
189 °C.<sup>11,13</sup> In comparison, pure GF starts to dissociate at 420

190 °C.<sup>34,47</sup> For the mixture of GO and GF with the 1:1 mass ratio, 190  
its first exothermic peak (first  $\Delta H$  in Figure 2b) starts around 191  
200 °C, similar to GO, and the second exotherm (second  $\Delta H$  192  
in Figure 2b) starts at  $\sim 400$  °C, which is earlier than both the 193  
second exothermic (oxidation) peak of GO and the 194  
dissociation peak of GF. Additionally, the residual mass 195  
fraction for GO/GF is 12.6% at 800 °C after all the reactions 196  
end, which is smaller than the average of pure GO and GF 197  
( $\sim 18.2\% = (26.3\% + 10.1\%)/2$ ), suggesting that more GO and 198  
GF have reacted to form gaseous products. Similarly, the 199  
amount of heat release integrated from the second exotherm 200  
(second  $\Delta H$  in Figure 2b) in GO/GF (9.36 kJ/g) is larger 201  
than those in GO and GF (8.58 and 7.50 kJ/g, respectively), as 202  
shown in Figure 2c. In summary, the GO/GF mixture 203  
produces more gaseous products and releases more heat than 204  
the average values of two separated components, indicating a 205  
synergistic effect between GO and GF. 206

Similar to the TGA/DSC observations, the fast-heating T- 207  
jump time-of-flight mass spectrometry (TOFMS) experiments 208  
also show a synergistic effect between GO and GF (Figure 2d). 209  
The T-jump experiments provide onset temperatures for both 210  
C<sub>x</sub>O<sub>y</sub> species (e.g., CO<sub>2</sub>, CO, C, and O) and CF<sub>x</sub> species. First, 211  
pure GO has an onset temperature for C<sub>x</sub>O<sub>y</sub> of 373 ± 50 °C. 212  
Most of the signal for C<sub>x</sub>O<sub>y</sub> comes from the thermal reaction/ 213  
decomposition product of the GO sample, and a small portion 214  
of C and O ion signals are from the fragmentation of CO<sub>2</sub> and/ 215  
or CO; second, pure GF has only one onset temperature 216  
around 717 ± 50 °C, where mainly CF<sub>x</sub> species are released 217  
from the dissociation of GF, while a small amount of C<sub>x</sub>O<sub>y</sub> 218  
species are also detected resulting from the oxygen residue in 219  
the system. Finally, the mixture of GO/GF (50/50 wt %) has a 220  
similar onset temperature of 362 ± 50 °C for C<sub>x</sub>O<sub>y</sub> as GO, but 221  
the onset temperature for CF<sub>x</sub> (622 ± 50 °C) is about 95 °C 222  
lower than that of GF. This behavior is very similar to the 223  
TGA/DSC onset temperatures (Figure 2a,b). As such, both 224  
TGA/DSC and T-jump experiments confirm that the presence 225  
of GO facilitates the dissociation of GF. 226

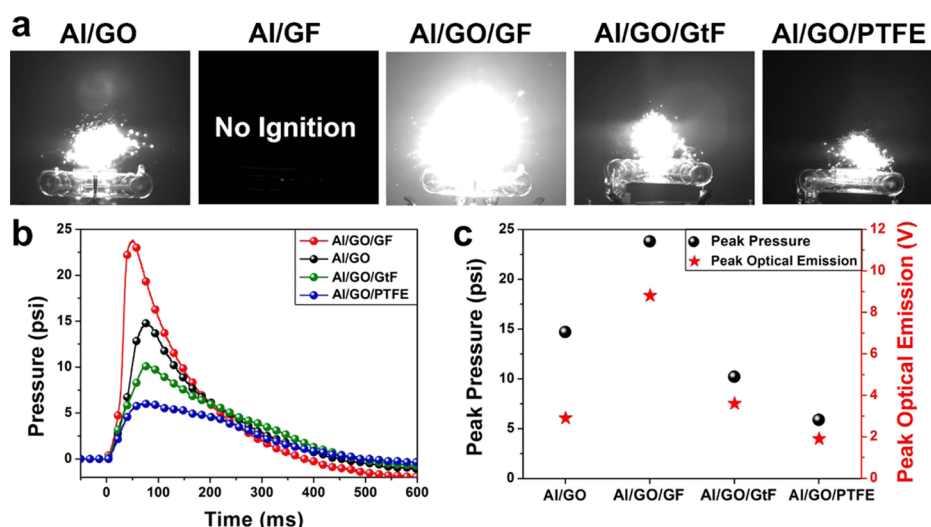


**Figure 4.** Comparison of the combustion performance of Al with different additives. (a) Snapshots of the burning of Al/GO (80/20 wt %), Al/GF (80/20 wt %), Al/GO/GF (80/10/10 wt %), Al/GO/GtF (80/10/10 wt %), and Al/GO/PTFE (80/10/10 wt %) composites at 40 ms after ignition by a Xe flash (power = 2.1 J/cm<sup>2</sup>); (b) traces of the time-resolved pressure release evolution and (c) summary of the peak values of pressure release and optical emission of aforementioned Al composites (except Al/GF) ignited in a constant-volume reactor by a Xe flash (power = 2.1 J/cm<sup>2</sup>).

### 3.2. RMD Simulations of Reaction Characteristics of GO, GF, and GO/GF Mixture in Air.

To understand the interaction between GO and GF at the molecular level, we performed RMD simulations to investigate the chemical evolution of GO, GF, and GO/GF (mass ratio of 1:1) in O<sub>2</sub> at 2000 K. Figure 3a–c provide snapshots of the GO, GF, and GO/GF systems at  $t = 0$  and 128 ps, respectively. At  $t = 128$  ps, the GO/GF mixture appears to have fewer larger GO and GF sheets and more small-sized species than both pure GO and GF systems, indicating a faster dissociation of the GO and/or GF sheets. Figure 3d compares the dynamic change of the relative potential energy, which is the interatomic potential energy change with respect to the initial potential energy of the system. It shows that the relative potential energy of the GO/GF mixture drops much faster than that of pure GO and GF (Figure 3d), indicating a faster energy release. It should be noted that the larger fluctuations in the potential energy evolution of the GF or GO/GF system (compared with the pure GO system) may be attributed to additional reaction steps of F–O, F–C, and F–H interactions in RMD simulations. A closer inspection of the RMD simulation results reveals the chemical reaction pathways for GO and GF. Figure 3e illustrates a few key reactions. GF dissociates at high temperatures and generates CF<sub>x</sub> radicals. CF<sub>x</sub> radicals can be oxidized by gaseous O<sub>2</sub> to produce O and CF<sub>x</sub>O<sub>y</sub> radicals, a radical branching reaction. CF<sub>x</sub> radicals can also be oxidized by O atoms on GO to form CF<sub>x</sub>O<sub>y</sub> radicals, which benefits both GF dissociation and GO disproportionation. Those RMD results suggest the molecular mechanisms on the experimentally observed synergistic interaction between GO and GF, which is caused by the accelerated radical generation and heat release.

**3.3. Experiential Comparison of  $\mu$ -Al Particle Combustion with GO, GF, GO/GF, and GO/Other Fluorinated Oxidizers as Additives.** The above studies of GO and GF without Al demonstrate the chemical and thermal couplings between GO and GF due to radical reactions. Next, we investigate how those couplings affect  $\mu$ -Al combustion by studying Al burning behavior to check the mechanism

illustrated in Figure 1. We choose five control samples, all at 80 wt % of  $\mu$ -Al particles with a diameter of 3.0–4.5  $\mu$ m and 20 wt % of additives. The five additives are GO (20 wt %), GF (20 wt %), GO/GF (10/10 wt %), GO/GtF (10/10 wt %), and GO/PTFE (10/10 wt %). The two other fluorine-containing additives, GtF and PTFE, were included for comparison with GF. GtF is the bulk form of GF and has been reported as an effective additive for metal combustion as aforementioned.<sup>26,27</sup> PTFE is a widely studied oxidizer for Al combustion.<sup>48</sup> All the samples were pressed into pellets with a packing porosity of  $\sim$ 83% and ignited by a Xe flash unit (AlienBees B1600). The experimental setup was illustrated in our previous work.<sup>11</sup> The flash pulse duration was about 5 ms and its integrated output power was about 2.1 J/cm<sup>2</sup>.

Figures 4a and S1 show the high-speed video snapshots of the burning process of those five samples. First, all samples, except Al/GF, can be ignited by the Xe flash lamp, indicating that GO is critical for the optical initiation due to its strong light absorption property. GF is transparent and cannot absorb much energy from the Xe flash lamp. Second, the Al/GO/GF (80/10/10 wt %) sample shows the most violent burning among all five samples. This suggests the synergistic benefits of GO/GF and also shows that GF exhibits a stronger enhancing effect for Al/GO combustion than GtF and PTFE. The comparison between Al/GO/GF and Al/GO/GtF implies that the ultrathin fluorinated graphene is more effective than the bulk fluorinated graphite, probably due to the higher specific surface area, finer dispersion, and easier access to F of GF. However, the performance of Al/GO/GF is also better than that of Al/GO/PTFE, suggesting that GF is superior to the popular PTFE to improve the energetic performance of Al.

Next, we quantitatively compare the burning properties of these five samples by determining their dynamic pressure–time traces measured in a constant-volume glass vial. The details of the burning experimental setup can be found in our previous works.<sup>11,49</sup> Briefly, 20 mg of sample powders were packed into a pellet with a porosity of  $\sim$ 83% in a 20 mL glass vial with ambient air inside. The vial was placed on top of the Xe flash unit, the samples were ignited at full power (2.1 J/



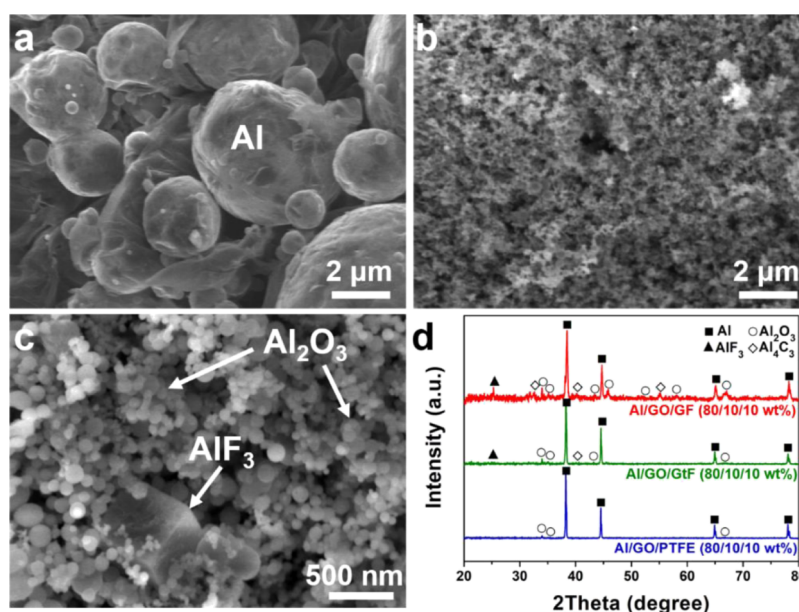


**Figure 5.** Characterization of the morphology and composition of the as-prepared sample and post-combustion products. SEM images of (a) the as-prepared Al/GO/GF (80/10/10 wt %), (b) its post-combustion products in the air, and (c) the enlarged image of (b); (d) XRD results of the post-combustion products in air of Al composites with GO and different fluorine-containing additives. The formation of  $\text{Al}_2\text{O}_3$  nanoparticles and  $\text{AlF}_3$  nanocubes is confirmed by combining SEM and XRD results.

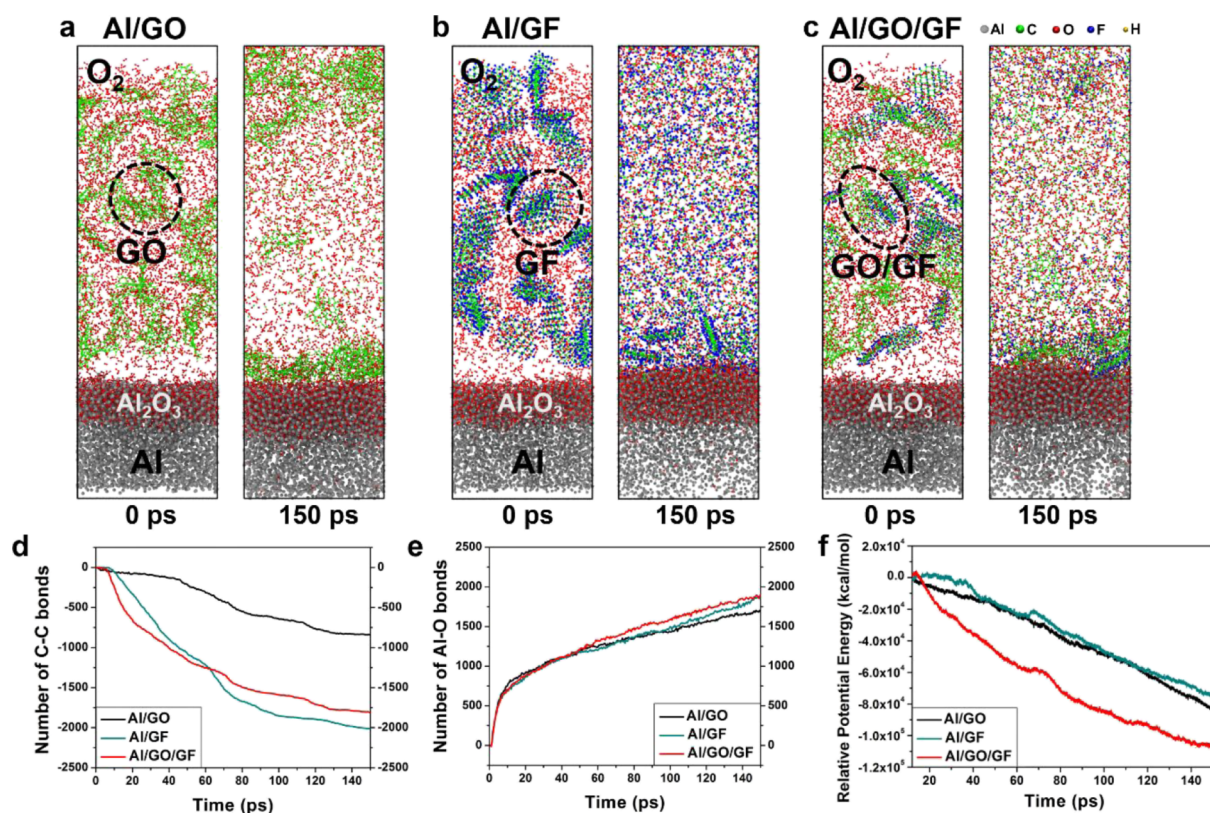


**Figure 6.** RMD simulation results reveal molecular-level thermal oxidation behaviors of Al/GO, Al/GF, and Al/GO/GF composites. Snapshots of RMD simulations of a pre-oxidized Al slab with (a) GO, (b) GF, and (c) GO/GF 1:1 mixture with  $\text{O}_2$  at 2500 K at  $t = 0$  and 150 ps (gray, Al atoms; green, C atoms; red, O atoms; blue, F atoms; yellow, H atoms); calculated number of (d) C–C bonds vs time and (e) Al–O bonds vs time; (f) the relative potential energy vs time. A lower relative potential energy indicates more heat release.

305  $\text{cm}^2$ ), and the time-resolved pressure and optical emission of  
 306 the vial were recorded by a pressure transducer (603B1, Kistler  
 307 Inc.) and a photodiode (PDA36A, Thorlabs Inc.). Figure 4b  
 308 shows the representative pressure–time traces of four control

samples, except Al/GF, since Al/GF cannot be ignited. The  
 309 peak pressures in Figure 4b and the peak optical intensity are  
 310 summarized in Figure 4c. The Al/GO/GF (80/10/10 wt %)   
 311 mixture exhibits the highest peak pressure, pressure rise rate,   
 312

313 and optical emission intensity, when compared with Al/GO,  
314 Al/GO/GtF, and Al/GO/PTFE samples. Even the Al/GO/  
315 GtF burns better than Al/GO/PTFE. Finally, the TGA/DSC  
316 results (Figure S2) of Al/GO (80/20 wt %) and Al/GO/GF  
317 (80/10/10 wt %) also demonstrate that Al/GO/GF has a  
318 higher specific heat release than Al/GO. The above results of  
319 pressure generation, optical emission, and heat release are  
320 consistent with the qualitative trend in the luminosity shown in  
321 Figures 4a and S1, indicating that the GO/GF is a more  
322 powerful additive than GO only for Al combustion.

### 3.4. Characterization of Al/GO/GF Post-Combustion

324 **Products.** The post-combustion products of Al/GO/GF  
325 (from constant-volume pressure test) were further charac-  
326 terized to understand the combustion process. Figure 5a–c  
327 show the scanning electron microscopy (SEM) images of the  
328 as-prepared Al/GO/GF composites and corresponding post-  
329 combustion products. The as-prepared sample contains  
330 spherical Al particles with an average diameter of 3–4.5  $\mu\text{m}$ ,  
331 and the Al particles appear to be wrapped by GO and GF  
332 sheets. After flash ignition and combustion, the combustion  
333 products are porous and composed of mainly spherical  
334 nanoparticles (Figure 5b,c), which are supposed to be  $\text{Al}_2\text{O}_3$ .  
335 There are some sub-micron-sized cubes in the products  
336 (Figure 5c), which contains both Al and F according to the  
337 element mapping from energy-dispersive X-ray spectroscopy  
338 (EDXS), as shown in Figure S3. Additionally, X-ray diffraction  
339 (XRD) spectra show the crystalline phase compositions within  
340 the products (Figure 5d). The main products are  $\text{Al}_2\text{O}_3$  and  
341  $\text{Al}_4\text{C}_3$  for all Al composites with GO and different fluorine-  
342 containing additives. The Al/GO/GF sample shows an  
343 obvious peak of  $\text{AlF}_3$ . The formation of  $\text{AlF}_3$  cubes is  
344 confirmed by both SEM/EDXS and XRD, which was also  
345 observed by previous studies on Al reaction with fluoropol-  
346 ymers.<sup>50,51</sup> The formation of  $\text{AlF}_3$  suggests that fluorine from  
347 GF reacts with Al and the fluorination of Al is one of the  
348 reasons for the enhanced performance of the Al/GO/GF  
349 sample.

### 3.5. RMD Simulations of $\mu$ -Al Oxidation with GO, GF, and GO/GF as Additives.

350 To understand the effect of GO/  
351 GF interaction on  $\mu$ -Al combustion at the molecular level, we  
352 conducted RMD simulations for three systems: Al/GO, Al/  
353 GF, and Al/GO/GF. Each system has a total number of 13,414  
354 atoms, including a pre-oxidized Al slab and 2000  $\text{O}_2$  molecules.  
355 In addition, the Al/GO system contains 32 GO sheets; the Al/  
356 GF system contains 32 GF sheets; the Al/GO/GF system  
357 contains 16 GO sheets and 16 GF sheets. We exposed each  
358 system to 2500 K at  $t = 0$  ps and let the system evolve until  $t =$   
359 150 ps. Figure 6a–c show snapshots of the Al/GO, Al/GF, and  
360 Al/GO/GF systems at  $t = 0$  and 150 ps, respectively. At  $t =$   
361 150 ps, the Al/GO/GF system appears to have fewer larger  
362 GO and GF sheets than both Al/GO and Al/GF system,  
363 similar to the cases without Al (Figure 3a–c). The number of  
364 broken C–C bonds in Al/GO/GF (1818 at  $t = 150$  ps) is also  
365 larger than the average value of those in Al/GO and Al/GF  
366 [(839 + 2013)/2 = 1426 at  $t = 150$  ps] (Figure 6d), which  
367 implies that more GO disproportionation/oxidation and GF  
368 dissociation occurred in Al/GO/GF. The Al/GF system  
369 (Figure 6b) shows a higher degree of dissociation (e.g., more  
370 C–C bonds break) and Al oxidation (e.g., more Al–O bonds  
371 formation) than the Al/GO system (Figure 6e), but a similar  
372 energy release as the Al/GO composites (Figure 6f). These  
373 results imply that the  $\text{CF}_x$  and  $\text{CF}_x\text{O}_y$  species released/oxidized  
374 from GF facilitate Al oxidation/fluorination, but the dissoci-

375 ation and oxidation of GF are not as exothermic as the  
376 disproportionation and oxidation of GO, which is also  
377 consistent with the thermal analysis (Figure 2b,c). Interest-  
378 ingly, the relative potential energy in the Al/GO/GF mixture  
379 drops the fastest (Figure 6f), yielding the highest amount of  
380 energy release among the three systems. This suggests that the  
381 Al/GO/GF system reacts faster and releases more heat than  
382 Al/GO and Al/GF (Figures 6d–f and S4a–c for comparison). 383

384 These trends in the RMD simulations agree with our  
385 experimental observations. The energetic performance of Al  
386 particles is effectively enhanced with the mixture of the GO/  
387 GF sheets. Replacing the GO sheets with the GF sheets does  
388 not greatly improve the combustion of the Al particles. Only  
389 when both GO and GF are present, the ejected  $\text{CF}_x$  species  
390 could react with the GO sheets, in addition to  $\text{O}_2$ , to produce  
391 more  $\text{CF}_x\text{O}_y$  to react with Al, forming Al–O bonds faster  
392 (Figures 6e and S4). 393

## 4. CONCLUSIONS

394 In summary, we conducted both experimentally thermal  
395 analysis and RMD simulations to investigate the synergistic  
396 chemical and thermal interactions between GO and GF. The  
397 dissociation of GF generates  $\text{CF}_x$  species, which are readily  
398 oxidized by GO, forming  $\text{CF}_x\text{O}_y$  radicals. In other words, GO  
399 reacts with GF through radical reactions that facilitate the  
400 breakdown of GF and GO to release heat more rapidly. Since  
401 the interaction between GO and GF generates oxidative  
402 radicals and heat, this coupling was further used to accelerate  
403 the combustion (i.e., oxidation) process of  $\mu$ -Al particles. We  
404 found that the Al/GO/GF composites exhibit improved  
405 energetic properties in terms of higher and faster pressure  
406 generation and stronger optical emission than Al/GO, Al/GF,  
407 and Al/GO/other fluorine-containing nanomaterials. These  
408 results demonstrate a new direction of utilizing chemical and  
409 thermal coupling reactions between ultrathin carbon materials  
410 to accelerate the combustion of Al and potentially oxidation  
411 reactions of other materials. 412

## ASSOCIATED CONTENT

### Supporting Information

413 The Supporting Information is available free of charge at  
414 <https://pubs.acs.org/doi/10.1021/acsami.9b20397>. 415

416 Time-resolved high-speed images showing the burning  
417 behaviors of Al composites; TGA/DSC results of Al/  
418 GO and Al/GO/GF composites; SEM/EDXS images of  
419 post-combustion products of Al/GO/GF composites in  
420 air; and evolutions of bond populations of Al/GO, Al/  
421 GF, and Al/GO/GF composites during RMD simu-  
422 lations (PDF) 423

## AUTHOR INFORMATION

### Corresponding Author

424 Xiaolin Zheng – Department of Mechanical Engineering,  
425 Stanford University, Stanford, California 94305, United States;  
426 [orcid.org/0000-0002-8889-7873](https://orcid.org/0000-0002-8889-7873); Email: [xlzheng@stanford.edu](mailto:xlzheng@stanford.edu) 427

### Authors

428 Yue Jiang – Department of Mechanical Engineering, Stanford  
429 University, Stanford, California 94305, United States;  
430 [orcid.org/0000-0002-6017-8551](https://orcid.org/0000-0002-6017-8551) 431



432 **Sili Deng** – Department of Mechanical Engineering, Stanford  
433 University, Stanford, California 94305, United States;  
434 Department of Mechanical Engineering, Massachusetts Institute  
435 of Technology, Cambridge, Massachusetts 02139, United  
436 States; [orcid.org/0000-0002-3421-7414](https://orcid.org/0000-0002-3421-7414)

437 **Sungwook Hong** – Collaboratory for Advanced Computing and  
438 Simulations, Department of Physics & Astronomy, Department  
439 of Computer Science, Department of Chemical Engineering &  
440 Materials Science, and Department of Biological Sciences,  
441 University of Southern California, Los Angeles, California  
442 90089, United States; Department of Physics and Engineering,  
443 California State University, Bakersfield, Bakersfield, California  
444 93311, United States; [orcid.org/0000-0003-3569-7701](https://orcid.org/0000-0003-3569-7701)

445 **Subodh Tiwari** – Collaboratory for Advanced Computing and  
446 Simulations, Department of Physics & Astronomy, Department  
447 of Computer Science, Department of Chemical Engineering &  
448 Materials Science, and Department of Biological Sciences,  
449 University of Southern California, Los Angeles, California  
450 90089, United States; [orcid.org/0000-0002-5516-6900](https://orcid.org/0000-0002-5516-6900)

451 **Haihan Chen** – Department of Chemical and Environmental  
452 Engineering, University of California, Riverside, Riverside,  
453 California 92507, United States

454 **Ken-ichi Nomura** – Collaboratory for Advanced Computing  
455 and Simulations, Department of Physics & Astronomy,  
456 Department of Computer Science, Department of Chemical  
457 Engineering & Materials Science, and Department of Biological  
458 Sciences, University of Southern California, Los Angeles,  
459 California 90089, United States

460 **Rajiv K. Kalia** – Collaboratory for Advanced Computing and  
461 Simulations, Department of Physics & Astronomy, Department  
462 of Computer Science, Department of Chemical Engineering &  
463 Materials Science, and Department of Biological Sciences,  
464 University of Southern California, Los Angeles, California  
465 90089, United States

466 **Aiichiro Nakano** – Collaboratory for Advanced Computing and  
467 Simulations, Department of Physics & Astronomy, Department  
468 of Computer Science, Department of Chemical Engineering &  
469 Materials Science, and Department of Biological Sciences,  
470 University of Southern California, Los Angeles, California  
471 90089, United States; [orcid.org/0000-0003-3228-3896](https://orcid.org/0000-0003-3228-3896)

472 **Priya Vashishta** – Collaboratory for Advanced Computing and  
473 Simulations, Department of Physics & Astronomy, Department  
474 of Computer Science, Department of Chemical Engineering &  
475 Materials Science, and Department of Biological Sciences,  
476 University of Southern California, Los Angeles, California  
477 90089, United States; [orcid.org/0000-0003-4683-429X](https://orcid.org/0000-0003-4683-429X)

478 **Michael R. Zachariah** – Department of Chemical and  
479 Environmental Engineering, University of California, Riverside,  
480 Riverside, California 92507, United States; [orcid.org/0000-0002-4115-3324](https://orcid.org/0000-0002-4115-3324)

482 Complete contact information is available at:  
483 <https://pubs.acs.org/10.1021/acsami.9b20397>

#### 484 Author Contributions

485 <sup>#</sup>Y.J., S.D. and S.H. contributed equally to this work.

#### 486 Notes

487 The authors declare no competing financial interest.

#### 488 ACKNOWLEDGMENTS

489 X.Z. acknowledges the support by the Office of Naval  
490 Research, under award number N00014-19-1-2085. The  
491 work at the University of Southern California was supported

as part of the Computational Materials Sciences Program 492  
funded by the U.S. Department of Energy, Office of Science, 493  
Basic Energy Sciences, under award number DE-SC0014607. 494  
The simulations were performed at the Argonne Leadership 495  
Computing Facility under the DOE INCITE and Aurora Early 496  
Science programs and at the Center for High Performance 497  
Computing of the University of Southern California. M.R.Z. 498  
and H.C. gratefully acknowledge support from the Army 499  
Research Office. 500

#### 501 REFERENCES

- (1) Rossi, C.; Zhang, K.; Esteve, D.; Alphonse, P.; Tailhades, P.; Vahlas, C. Nanoenergetic Materials for MEMS: A Review. *J. Microelectromech. Syst.* **2007**, *16*, 919–931. 502
- (2) Yetter, R. A.; Risha, G. A.; Son, S. F. Metal Particle Combustion and Nanotechnology. *Proc. Combust. Inst.* **2009**, *32*, 1819–1838. 503
- (3) He, W.; Liu, P.-J.; He, G.-Q.; Gozin, M.; Yan, Q.-L. Highly Reactive Metastable Intermixed Composites (MICs): Preparation and Characterization. *Adv. Mater.* **2018**, *30*, 1706293. 504
- (4) Wang, J.; Jiang, X.; Zhang, L.; Qiao, Z.; Gao, B.; Yang, G.; Huang, H. Design and Fabrication of Energetic Superlattice Like-PTFE/Al with Superior Performance and Application in Functional Micro-initiator. *Nano Energy* **2015**, *12*, 597–605. 505
- (5) Yang, M.; Liu, J.; Li, S.; Zhang, S.; Wang, Y.; He, C. Ultrafast Synthesis of Graphene Nanosheets Encapsulated Si Nanoparticles via Deflagration of Energetic Materials for Lithium-Ion Batteries. *Nano Energy* **2019**, *65*, 104028. 506
- (6) Comet, M.; Martin, C.; Schnell, F.; Spitzer, D. Nanothermites: A Short Review. Factsheet for Experimenters, Present and Future Challenges. *Propellants, Explos., Pyrotech.* **2019**, *44*, 18–36. 507
- (7) Brooks, K. P.; Beckstead, M. W. Dynamics of Aluminum Combustion. *J. Propul. Power* **1995**, *11*, 769–780. 508
- (8) Huang, Y.; Risha, G. A.; Yang, V.; Yetter, R. A. Effect of Particle Size on Combustion of Aluminum Particle Dust in Air. *Combust. Flame* **2009**, *156*, 5–13. 509
- (9) Sundaram, D.; Yang, V.; Yetter, R. A. Metal-Based Nano-energetic Materials: Synthesis, Properties, and Applications. *Prog. Energy Combust. Sci.* **2017**, *61*, 293–365. 510
- (10) Dreizin, E. L. Metal-Based Reactive Nanomaterials. *Prog. Energy Combust. Sci.* **2009**, *35*, 141–167. 511
- (11) Jiang, Y.; Deng, S.; Hong, S.; Zhao, J.; Huang, S.; Wu, C.-C.; Gottfried, J. L.; Nomura, K.-i.; Li, Y.; Tiwari, S.; Kalia, R. K.; Vashishta, P.; Nakano, A.; Zheng, X. Energetic Performance of Optically Activated Aluminum/Graphene Oxide Composites. *ACS Nano* **2018**, *12*, 11366–11375. 512
- (12) Sabourin, J. L.; Dabbs, D. M.; Yetter, R. A.; Dryer, F. L.; Aksay, I. A. Functionalized Graphene Sheet Colloids for Enhanced Fuel/Propellant Combustion. *ACS Nano* **2009**, *3*, 3945–3954. 513
- (13) Krishnan, D.; Kim, F.; Luo, J.; Cruz-Silva, R.; Cote, L. J.; Jang, H. D.; Huang, J. Energetic Graphene Oxide: Challenges and Opportunities. *Nano today* **2012**, *7*, 137–152. 514
- (14) Thiruvengadathan, R.; Staley, C.; Geeson, J. M.; Chung, S.; Raymond, K. E.; Gangopadhyay, K.; Gangopadhyay, S. Enhanced Combustion Characteristics of Bismuth Trioxide-Aluminum Nanocomposites Prepared through Graphene Oxide Directed Self-Assembly. *Propellants, Explos., Pyrotech.* **2015**, *40*, 729–734. 515
- (15) Gilje, S.; Dubin, S.; Badakhshan, A.; Farrar, J.; Danczyk, S. A.; Kaner, R. B. Photothermal Deoxygenation of Graphene Oxide for Patterning and Distributed Ignition Applications. *Adv. Mater.* **2010**, *22*, 419–423. 516
- (16) Li, X.; Huang, B.; Li, R.; Zhang, H. p.; Qin, W.; Qiao, Z.; Liu, Y.; Yang, G. Laser-Ignited Relay-Domino-Like Reactions in Graphene Oxide/CL-20 Films for High-Temperature Pulse Preparation of Bi-Layered Photothermal Membranes. *Small* **2019**, *15*, 1900338. 517
- (17) Cote, L. J.; Cruz-Silva, R.; Huang, J. Flash Reduction and Patterning of Graphite Oxide and Its Polymer Composite. *J. Am. Chem. Soc.* **2009**, *131*, 11027–11032. 518



- 558 (18) Crouse, C. A. Fluorinated Polymers as Oxidizers for Energetic  
559 Composites. *Advances in Fluorine-Containing Polymers*; American  
560 Chemical Society, 2012; Vol. 1106, pp 127–140.
- 561 (19) Kappagantula, K. S.; Farley, C.; Pantoya, M. L.; Horn, J. Tuning  
562 Energetic Material Reactivity Using Surface Functionalization of  
563 Aluminum Fuels. *J. Phys. Chem. C* **2012**, *116*, 24469–24475.
- 564 (20) Huang, S.; Pan, M.; Deng, S.; Jiang, Y.; Zhao, J.; Levy-Wendt,  
565 B.; Tang, S. K. Y.; Zheng, X. Modified Micro-Emulsion Synthesis of  
566 Highly Dispersed Al/PVDF Composites with Enhanced Combustion  
567 Properties. *Adv. Eng. Mater.* **2019**, *21*, 1801330.
- 568 (21) McCollum, J.; Pantoya, M. L.; Iacono, S. T. Activating  
569 Aluminum Reactivity with Fluoropolymer Coatings for Improved  
570 Energetic Composite Combustion. *ACS Appl. Mater. Interfaces* **2015**,  
571 *7*, 18742–18749.
- 572 (22) Watson, K. W.; Pantoya, M. L.; Levitas, V. I. Fast Reactions  
573 with Nano- and Micrometer Aluminum: A Study on Oxidation versus  
574 Fluorination. *Combust. Flame* **2008**, *155*, 619–634.
- 575 (23) Kim, D. W.; Kim, K. T.; Min, T. S.; Kim, K. J.; Kim, S. H.  
576 Improved Energetic-Behaviors of Spontaneously Surface-Mediated Al  
577 Particles. *Sci. Rep.* **2017**, *7*, 4659.
- 578 (24) Row, S. L.; Groven, L. J. Smart Energetics: Sensitization of the  
579 Aluminum-Fluoropolymer Reactive System. *Adv. Eng. Mater.* **2018**,  
580 *20*, 1700409.
- 581 (25) Wang, H.; Shen, J.; Kline, D. J.; Eckman, N.; Agrawal, N. R.;  
582 Wu, T.; Wang, P.; Zachariah, M. R. Direct Writing of a 90 wt%  
583 Particle Loading Nanothermite. *Adv. Mater.* **2019**, *31*, 1806575.
- 584 (26) Koch, E.-C. Metal/fluorocarbon pyrolants: VI. Combustion  
585 Behaviour and Radiation Properties of Magnesium/Poly (Carbon  
586 Monofluoride) Pyrolant. *Propellants, Explos., Pyrotech.* **2005**, *30*, 209–  
587 215.
- 588 (27) Sippel, T. R.; Son, S. F.; Groven, L. J. Modifying Aluminum  
589 Reactivity with Poly(Carbon Monofluoride) via Mechanical Activa-  
590 tion. *Propellants, Explos., Pyrotech.* **2013**, *38*, 321–326.
- 591 (28) Feng, W.; Long, P.; Feng, Y.; Li, Y. Two-Dimensional  
592 Fluorinated Graphene: Synthesis, Structures, Properties and Applica-  
593 tions. *Adv. Sci.* **2016**, *3*, 1500413.
- 594 (29) Nair, R. R.; Ren, W.; Jalil, R.; Riaz, I.; Kravets, V. G.; Britnell,  
595 L.; Blake, P.; Schedin, F.; Mayorov, A. S.; Yuan, S.; Katsnelson, M. I.;  
596 Cheng, H.-M.; Strupinski, W.; Bulusheva, L. G.; Okotrub, A. V.;  
597 Grigorieva, I. V.; Grigorenko, A. N.; Novoselov, K. S.; Geim, A. K.  
598 Fluorographene: A Two-Dimensional Counterpart of Teflon. *Small*  
599 **2010**, *6*, 2877–2884.
- 600 (30) Liu, H. Y.; Hou, Z. F.; Hu, C. H.; Yang, Y.; Zhu, Z. Z.  
601 Electronic and Magnetic Properties of Fluorinated Graphene with  
602 Different Coverage of Fluorine. *J. Phys. Chem. C* **2012**, *116*, 18193–  
603 18201.
- 604 (31) Karlický, F.; Kumara Ramanatha Datta, K.; Otyepka, M.;  
605 Zbořil, R. Halogenated Graphenes: Rapidly Growing Family of  
606 Graphene Derivatives. *ACS Nano* **2013**, *7*, 6434–6464.
- 607 (32) Han, S. S.; Yu, T. H.; Merinov, B. V.; van Duin, A. C. T.;  
608 Yazami, R.; Goddard, W. A. Unraveling Structural Models of Graphite  
609 Fluorides by Density Functional Theory Calculations. *Chem. Mater.*  
610 **2010**, *22*, 2142–2154.
- 611 (33) Belenkov, M. E.; Chernov, V. M.; Belenkov, E. A. Structure of  
612 Fluorographene and Its Polymorphous Varieties. *J. Phys.: Conf. Ser.*  
613 **2018**, *1124*, 022010.
- 614 (34) Gong, P.; Wang, Z.; Wang, J.; Wang, H.; Li, Z.; Fan, Z.; Xu, Y.;  
615 Han, X.; Yang, S. One-Pot Sonochemical Preparation of Fluorogra-  
616 phene and Selective Tuning of Its Fluorine Coverage. *J. Mater. Chem.*  
617 **2012**, *22*, 16950–16956.
- 618 (35) Robinson, J. T.; Burgess, J. S.; Junkermeier, C. E.; Badescu, S.  
619 C.; Reinecke, T. L.; Perkins, F. K.; Zalalutdniov, M. K.; Baldwin, J.  
620 W.; Culbertson, J. C.; Sheehan, P. E.; Snow, E. S. Properties of  
621 Fluorinated Graphene Films. *Nano Lett.* **2010**, *10*, 3001–3005.
- 622 (36) Ohkura, Y.; Rao, P. M.; Zheng, X. Flash Ignition of Al  
623 Nanoparticles: Mechanism and Applications. *Combust. Flame* **2011**,  
624 *158*, 2544–2548.
- (37) Ohkura, Y.; Rao, P. M.; Sun Cho, I.; Zheng, X. Reducing 625  
Minimum Flash Ignition Energy of Al Microparticles by Addition of 626  
WO<sub>3</sub> Nanoparticles. *Appl. Phys. Lett.* **2013**, *102*, 043108. 627
- (38) Yang, F.; Zhang, Y.; Yang, X.; Zhong, M.; Yi, Z.; Liu, X.; Kang, 628  
X.; Luo, J.; Li, J.; Wang, C.-Y.; Zhao, H.-B.; Fu, Z.-B.; Tang, Y.-J. 629  
Enhanced Photothermal Effect in Ultralow-Density Carbon Aerogels 630  
with Microporous Structures for Facile Optical Ignition Applications. 631  
*ACS Appl. Mater. Interfaces* **2019**, *11*, 7250–7260. 632
- (39) Zhou, L.; Piekiet, N.; Chowdhury, S.; Zachariah, M. R. T- 633  
Jump/Time-of-Flight Mass Spectrometry for Time-Resolved Analysis 634  
of Energetic Materials. *Rapid Commun. Mass Spectrom.* **2009**, *23*, 635  
194–202. 636
- (40) van Duin, A. C. T.; Dasgupta, S.; Lorant, F.; Goddard, W. A. 637  
ReaxFF: A Reactive Force Field for Hydrocarbons. *J. Phys. Chem. A* 638  
**2001**, *105*, 9396–9409. 639
- (41) Senftle, T. P.; Hong, S.; Islam, M. M.; Kylasa, S. B.; Zheng, Y.; 640  
Shin, Y. K.; Junkermeier, C.; Engel-Herbert, R.; Janik, M. J.; Aktulga, 641  
H. M. The ReaxFF Reactive Force-Field: Development, Applications 642  
and Future Directions. *npj Comput. Mater.* **2016**, *2*, 15011. 643
- (42) Hong, S.; van Duin, A. C. T. Atomistic-Scale Analysis of 644  
Carbon Coating and Its Effect on the Oxidation of Aluminum 645  
Nanoparticles by ReaxFF-Molecular Dynamics Simulations. *J. Phys.* 646  
*Chem. C* **2016**, *120*, 9464–9474. 647
- (43) Rahnamoun, A.; van Duin, A. C. T. Reactive Molecular 648  
Dynamics Simulation on the Disintegration of Kapton, POSS 649  
Polyimide, Amorphous Silica, and Teflon During Atomic Oxygen 650  
Impact Using the ReaxFF Reactive Force-Field Method. *J. Phys. Chem.* 651  
*A* **2014**, *118*, 2780–2787. 652
- (44) Kim, S.-Y.; van Duin, A. C. T.; Kubicki, J. D. Molecular 653  
Dynamics Simulations of the Interactions between TiO<sub>2</sub> Nano- 654  
particles and Water with Na<sup>+</sup> and Cl<sup>-</sup>, Methanol, and Formic Acid 655  
Using a Reactive Force Field. *J. Mater. Res.* **2013**, *28*, 513–520. 656
- (45) Nosé, S. A Unified Formulation of the Constant Temperature 657  
Molecular Dynamics Methods. *J. Chem. Phys.* **1984**, *81*, 511–519. 658
- (46) Hoover, W. G. Canonical Dynamics: Equilibrium Phase-Space 659  
Distributions. *Phys. Rev. A: At, Mol., Opt. Phys.* **1985**, *31*, 1695. 660
- (47) Wang, X.; Dai, Y.; Wang, W.; Ren, M.; Li, B.; Fan, C.; Liu, X. 661  
Fluorographene with High Fluorine/Carbon Ratio: A Nanofiller for 662  
Preparing Low- $\kappa$  Polyimide Hybrid Films. *ACS Appl. Mater. Interfaces* 663  
**2014**, *6*, 16182–16188. 664
- (48) Collins, E. S.; Skelton, B. R.; Pantoya, M. L.; Irin, F.; Green, M. 665  
J.; Daniels, M. A. Ignition Sensitivity and Electrical Conductivity of 666  
An Aluminum Fluoropolymer Reactive Material with Carbon 667  
Nanofillers. *Combust. Flame* **2015**, *162*, 1417–1421. 668
- (49) Huang, S.; Deng, S.; Jiang, Y.; Zheng, X. Experimental Effective 669  
Metal Oxides to Enhance Boron Combustion. *Combust. Flame* **2019**, 670  
*205*, 278–285. 671
- (50) Wang, H.; Kline, D. J.; Rehwoldt, M.; Wu, T.; Zhao, W.; Wang, 672  
X.; Zachariah, M. R. Architecture Can Significantly Alter the Energy 673  
Release Rate from Nanocomposite Energetics. *ACS Appl. Polym.* 674  
*Mater.* **2019**, *1*, 982–989. 675
- (51) Kostoglou, N.; Emre Gunduz, I.; Isik, T.; Ortalan, V.; 676  
Constantinides, G.; Kontos, A. G.; Steriotis, T.; Ryzhkov, V.; 677  
Bousser, E.; Matthews, A.; Doumanidis, C.; Mitterer, C.; Rebholz, 678  
C. Novel Combustion Synthesis of Carbon Foam-Aluminum Fluoride 679  
Nanocomposite Materials. *Mater. Des.* **2018**, *144*, 222–228. 680